JOURNAL OF MAGNETIC RESONANCE **132,** 260–265 (1998)
ARTICLE NO. MN981410

# A Generalized Estimate of the SLR *B* Polynomial Ripples for RF Pulse Generation

A. Raddi and U. Klose

*Department of Neuroradiology, University of Tübingen, Hoppe-Seyler Strasse 3, D-72076 Tübingen, Germany*

E-mail: antonella.raddi@med.uni-tuebingen.de

Received April 2, 1997; revised November 20, 1997

**The nonlinearity of the parameter relations for the Shinnar–Le Roux RF pulse design algorithm has induced to perform a classification based on the features of the slice profile due to the RF pulse. In the present paper a generalization of the relation between the ripple amplitudes of the SLR *B* polynomial and those of the slice profile is given. It allows generation of RF pulses with better slice profiles and slightly reduced energy, avoiding any *a priori* classification. The effect of our estimation has been shown by generating several pulses by generalized estimation of *B* polynomial ripples. In addition, their behavior has been compared to that of analogous pulses generated by means of the classification just mentioned.** 

The Shinnar–Le Roux (SLR) algorithm (*1–5*) reduces the RF pulse design problem to the design of two polynomials: *A* and *B*. Given a couple of polynomials, in fact, the SLR algorithm permits their conversion into an RF pulse waveform. The polynomials *A* and *B* have to satisfy appropriate constraints in order to optimally approximate the desired slice profile, whose parameters—the passband and stopband edges, and the in-slice and out-of-slice ripples—have to be specified.

Shinnar and Leigh (*4*) and Le Roux (*5*) proved the existence of the polynomials and established a relation between them and the magnetization vector. Because of the nonlinearity of such a relation, it is impossible to perform a direct calculation of the polynomials' parameters (*6*). Therefore, an approximation is required.

Based on experimental measurements, Rabiner and Gold (*7*) obtained a set of empirical relations between the passband and stopband edges, and the in-slice and out-of-slice ripples. For this reason, the attention has been focused only on the estimate of the ripple amplitudes (*6*).

Pauly *et al.* (*6*) carried out the approximation of ripple amplitudes for five types of pulses: small flip angle, $\pi/2$ excitation, $\pi$ inversion, $\pi$ crushed spin echo, $\pi/2$ saturation. In the Matpulse-1.0 implementation of the SLR algorithm, Matson (*8*) performed a classification of RF pulses, based on the RF types of Pauly, the flip angle, the initial orientation of the magnetization vector, and the parameter of interest: transverse or longitudinal magnetization.

Such a classification has more than one drawback. First, it forces the performance of an *a priori* choice about the initial magnetization vector and the parameter of interest. Furthermore, the *B* polynomial ripples are estimated only for those five types of pulses. In all of the other cases, according to the class of pulses, the same estimation is used, damaging the quality of the slice profiles, especially for the $\pi/2$ excitation class.

In order to avoid any initial classification, we have performed a generalization of the estimate of the relations between the *B* polynomial and the slice profile ripple amplitudes, which allows generating RF pulses just by setting their flip angle.

## THE SHINNAR–LE ROUX ALGORITHM: FORWARD TRANSFORM

In the Schrödinger representation, if the terms related to relaxation time are neglected, the Bloch equation reduces to a rotation, which can be described through a *spinor* $(\alpha, \beta)$.

Here

$$\alpha = \cos(\phi/2) - in_z\sin(\phi/2) \quad [1]$$

$$\beta = -i(n_x + in_y)\sin(\phi/2) \quad [2]$$

are determined by the rotation angle $\phi$ and the rotation axis $\mathbf{n} = (n_x, n_y, n_z)$. The spin vector $(\alpha, \beta)$ satisfies the constrain $\alpha\alpha^* + \beta\beta^* = 1$.

After the application of an RF field and a magnetic field gradient, the solution to the Bloch equation can be written as

$$\begin{pmatrix} M_{xy}^{+} \\ M_{xy}^{+*} \\ M_z^{+} \end{pmatrix} = \begin{pmatrix} (\alpha^*)^2 & -\beta^2 & 2\alpha^*\beta \\ -(\beta^*)^2 & \alpha^2 & 2\alpha\beta^* \\ -\alpha^*\beta^* & -\alpha\beta & 1 - 2\beta\beta^* \end{pmatrix} \begin{pmatrix} M_{xy}^{-} \\ M_{xy}^{-*} \\ M_z^{-} \end{pmatrix}, \quad [3]$$

where $M_z$ and $M_{xy} = M_x + iM_y$ stand for longitudinal and transverse magnetization, and the superscripts + and − refer to the magnetization after and before the application of the field



1090-7807/98 $25.00

**TABLE 1**
**Standard Relationships for Ripple Amplitudes**

| Pulse | Parameter of interest | $\delta_1$ | $\delta_2$ |
|---|---|---|---|
| Small-tip-angle | $M_{xy}$ | $\delta_1^e$ | $\delta_2^e$ |
| $\pi/2$ selective excitation | $M_{xy}$ | $\sqrt{\delta_1^e/2}$ | $\delta_2^e/\sqrt{2}$ |
| $\pi$ inversion | $M_z$ | $\delta_1^e/8$ | $\sqrt{\delta_2^e/2}$ |
| Crushed spin-echo | $M_{xy}$ | $\delta_1^e/4$ | $\sqrt{\delta_2^e}$ |
| Saturation | $M_z$ | $\delta_1^e/2$ | $\sqrt{\delta_2^e}$ |

(* denotes complex conjugation). If a sequence of $n$ pulses is applied, the overall rotation can be represented as the product of the $n$ individual rotations.

Under the hard-pulse approximation, the RF pulse $\mathbf{H}_1$ is made up of $n$ constant sample $\mathbf{H}_{1,j}$ with a duration $\Delta t$. If a piecewise RF pulse is combined with a field gradient whose amplitude is $G$, the rotation parameters—flip angle $\phi_j$ and rotation axis $\mathbf{n}_j$—can be calculated by

$$\phi_j = -\gamma\Delta t\sqrt{|\mathbf{H}_{1,j}|^2 + (Gx)^2}$$
$$\mathbf{n}_j = \frac{\gamma\Delta t}{|\phi_j|}(H_{1,x,j}, H_{1,y,j}, Gx),$$

where $\gamma$ is the gyromagnetic ratio.

The SLR key hypothesis (*4–6*) is that it is possible to separate the rotation due to the field gradient from the rotation of the magnetization due to the RF pulse, if the flip angle $\phi_j = -\gamma\Delta t|\mathbf{H}_{1,j}|$ is small for every $j = 1, \ldots, n$. At every step, the overall rotation can be described by the product of the two spinors $(z, 0)$, for the field gradient, and $(C_j, S_j)$, for the RF field:

$$(z, 0) = (e^{i\gamma Gx\Delta t}, 0)$$
$$(C_j, S_j) = (\cos(\phi_j/2), ie^{i(\theta_{1,j})}\sin(\phi_j/2)).$$

The angle $\theta_j$ stands for the phase of $\mathbf{H}_{1,j}$.

The net effect of the sequence $(C_j, S_j)(z, 0)(C_{j-1}, S_{j-1})(z, 0)\cdots(C_0, S_0)(z, 0)$ is represented by the spinor $(\alpha_j, \beta_j)$ that can be iteratively calculated by

$$\begin{pmatrix}\alpha_j\\ \beta_j\end{pmatrix} = \begin{pmatrix} C_j & -S_j^* \\ S_j & C_j^*\end{pmatrix}\begin{pmatrix} z^{1/2} & 0 \\ 0 & z^{-1/2}\end{pmatrix}\begin{pmatrix}\alpha_{j-1}\\ \beta_{j-1}\end{pmatrix}.$$

The replacement of $\alpha_j$ and $\beta_j$ with

$$A_j = z^{-j/2}\alpha_j \quad [4]$$
$$B_j = z^{-j/2}\beta_j \quad [5]$$

allows the description of every spinor by a couple of $(j-1)$-order polynomials $A_j$ and $B_j$ which satisfy the constraint $|A_j(z)|^2 + |B_j(z)|^2 = 1$ for every $j = 1, \ldots, n$.

The spin vector $(\alpha, \beta)$ in Eq. [3] can be considered the result of the overall rotation, so it can be represented by the couple of polynomials $A_n$ and $B_n$. The solution to the Bloch equation then becomes

$$\begin{pmatrix}M_{xy}^+\\ M_{xy}^{+*}\\ M_z^+\end{pmatrix} = \begin{pmatrix} z^{-n}(A_n^*)^2 & -z^nB_n^2 & 2A_n^*B_n \\ -z^{-n}(B_n^*)^2 & z^nA_n^2 & 2A_nB_n^* \\ -z^{-n}A_n^*B_n^* & -z^nA_nB_n & 1-2B_nB_n^*\end{pmatrix}\begin{pmatrix}M_{xy}^-\\ M_{xy}^{-*}\\ M_z^-\end{pmatrix}. \quad [6]$$

## ESTIMATE OF *B* POLYNOMIAL RIPPLES BY MEANS OF A CLASSIFICATION

The nonlinearity of the relation between the parameters of the $B$ polynomial[1] and those characterizing the slice profile (see Eq. [6]) especially influences the relations between the ripple amplitude in $B$—$\delta_1$ (in-slice) and $\delta_2$ (out-of-slice)—and the effective slice profile ripples—$\delta_1^e$ and $\delta_2^e$.

Pauly *et al.* (*6*) derive the relations between the $B$ polynomial ripple amplitudes and those characterizing the slice profile for five types of pulses, combining the choice of the flip angle with appropriate initial magnetization and corresponding parameter.

Table 1 summarizes such relations, from now on called *standard.*

Matson (*8*) calculates the SLR $B$ polynomial ripples for every pulse, whose flip angle runs from 0° to 230°, using a classification based on a ''reference'' flip angle. Every RF pulse whose tip angle is in the range [45°, 135°], for instance, is classified as a ''$\pi/2$ excitation'' pulse. That means that the ripple amplitudes in the $B$ polynomial are calculated using the relation Pauly *et al.* derive for a 90° pulse, whatever the flip angle in [45°, 135°] is.

The implication is that the slice profiles simulated by using the pulses thus generated are not optimal.

## GENERALIZED ESTIMATE OF *B* POLYNOMIAL RIPPLES

We assume, for computational aims, that the initial magnetization is at the equilibrium, $\mathbf{M} \equiv (0, 0, 1)$, and that the applied RF pulse lies in the $xy$ plane, $\mathbf{n} \equiv (n_x, n_y, 0)$.

Under such hypotheses, Eqs. [1] and [2] reduce to

$$\alpha = \cos(\phi/2) \quad \beta = -i(n_x + in_y)\sin(\phi/2),$$

while Eq. [3] changes into

$$\mathbf{M}_{xy}^+ = 2\alpha^*\beta$$
$$\mathbf{M}_z^+ = 1 - 2\beta\beta^*.$$

[1] Henceforth, the subscripts will be used only if strictly necessary.

From Eq. [5] we can write the Cayley–Klein parameter $\beta$ as

$$\beta = z^{n/2}B(z)$$

and the amplitude of the transverse and longitudinal magnetization as

$$|\mathbf{M}_{xy}^{+}| = 2|\alpha^{*}B| = 2|\cos(\phi/2)\|B|$$
$$|\mathbf{M}_{z}^{+}| = |1 - 2BB^{*}| = |1 - 2|B|^{2}|$$
$$= \begin{cases} (1 - 2|B|^{2}), & \phi \in \left[0, \dfrac{\pi}{2}\right] \cup \left[\dfrac{3\pi}{2}, 2\pi\right] \\ (2|B|^{2} - 1), & \phi \in \left(\dfrac{\pi}{2}, \dfrac{3\pi}{2}\right) \end{cases}.$$

Neglecting the influence the $B$ polynomial ripples have on the cosine, the amplitude of the transverse magnetization depends linearly on $|B|$. In contrast, the amplitude of the longitudinal magnetization depends on $|B|$ in a quadratic manner.

If we use $|B| \pm \delta_k$ ($k = 1$ in-slice, $k = 2$ out-of-slice) instead of $|B|$ the amplitudes of the transverse and longitudinal magnetization vector become

$$|\mathbf{M}_{xy}^{+}| = 2|\cos(\phi/2)\|B| \pm 2|\cos(\phi/2)|\delta_k$$
$$|\mathbf{M}_{z}^{+}| = \begin{cases} 1 - 2(|B| \pm \delta_k)^{2} \approx 1 - 2|B|^{2} \\ \quad \pm 4\delta_k|B|, \quad \phi \in \left[0, \dfrac{\pi}{2}\right] \cup \left[\dfrac{3\pi}{2}, 2\pi\right] \\ (2|B| \pm \delta_k)^{2} - 1 \approx 2|B|^{2} - 1 \\ \quad \pm 4\delta_k|B|, \quad \phi \in \left(\dfrac{\pi}{2}, \dfrac{3\pi}{2}\right) \end{cases}.$$

For the transverse and the longitudinal magnetization, the relation between the effective ripple amplitudes of the magnetization $\delta_k^e$ and the B polynomial ripples $\delta_k$ can therefore be written as

$$\delta_{kxy}^{e} \approx 2|\cos(\phi/2)|\delta_k, \quad \delta_{kz}^{e} \approx 4|\sin(\phi/2)|\delta_k. \qquad [7]$$

In order to avoid choosing either the relations for the longitudinal magnetization or those for the transverse magnetization, it is possible to consider *weighted* values adding $\delta_{kxy}^{e}$ and $\delta_{kz}^{e}$, each respectively multiplied by the fraction of the transverse and longitudinal magnetization of the total magnetization $\mathbf{M}$:

$$\delta_k^{e} = \frac{|\mathbf{M}_{xy}|}{|\mathbf{M}|}\,\delta_{kxy}^{e} + \frac{|\mathbf{M}_{z}|}{|\mathbf{M}|}\,\delta_{kz}^{e}.$$

The magnetization is supposed to have unitary value; therefore, the previous equations become

$$\delta_k^{e} = |\sin(\phi)|\delta_{kxy}^{e} + |\cos(\phi)|\delta_{kz}^{e}. \qquad [8]$$

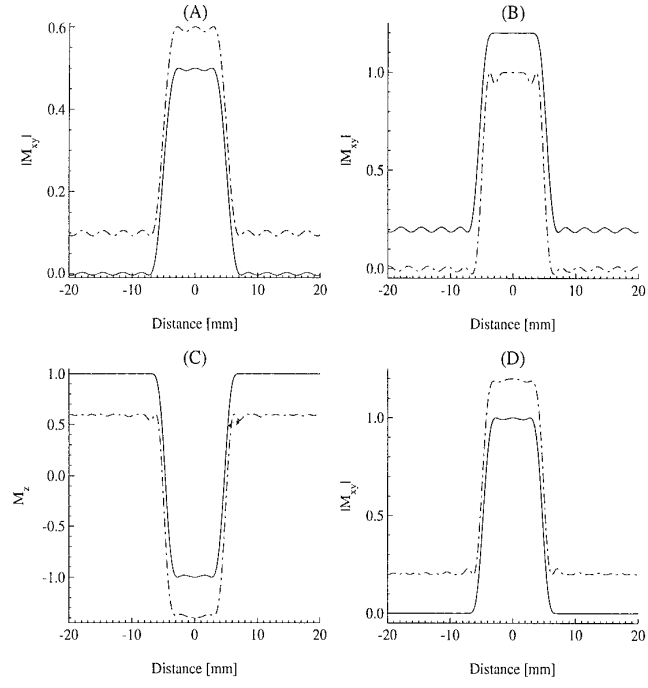


**FIG. 1.** Comparison between linear-phase pulses calculated using generalized (solid line) and standard (dash–dot line) estimate of the SLR $B$ polynomial ripples. Slice profiles due to 30° and 90° pulses are illustrated in (A) and (B), while the slice profiles due to 180° pulse used both as inversion and spin echo pulse are shown in (C) and (D).

Replacing $\delta_{kxy}^{e}$ and $\delta_{kz}^{e}$ with the values in Eqs. [7] and assuming that there is no reason to choose different values for the $B$ polynomial ripples according to the parameter of interest, Eq. [8] changes into

$$\delta_k^{e} = 2\delta_k\left(|\sin(\phi)\|\cos\left(\frac{\phi}{2}\right)| + 2|\cos(\phi)\|\sin\left(\frac{\phi}{2}\right)|\right). \qquad [9]$$

Equation [9] can be inverted

$$\delta_k = \frac{\delta_k^{e}}{2\left(|\sin(\phi)\|\cos\left(\frac{\phi}{2}\right)| + 2|\cos(\phi)\|\sin\left(\frac{\phi}{2}\right)|\right)},$$

allowing the calculation of the appropriate $B$ polynomial ripples once the effective slice profile ripple amplitudes have been set up.

## RESULTS AND DISCUSSION

In order to compare the slice profiles calculated using the standard classification to those designed using the generalized estimate of the SLR $B$ polynomial ripples, we generated two series of RF pulses—one for each type of estimation—with a duration of 3.072 ms and a bandwidth of 2 kHz, and with 1% in-slice and out-of-slice effective ripple amplitudes. A third

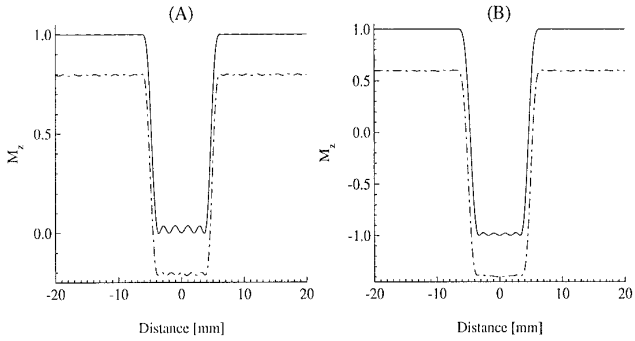


**FIG. 2.** Minimum-phase slice profiles produced by 90° saturation pulse (A) and by 180° inversion pulse (B). Generalized estimate (solid line), standard estimate (dash–dot line).

series of generalized estimate pulses with the same duration and bandwidth was generated with 5% out-of-slice ripple to reduce the transition band in the slice profile. In all cases we used 256 steps to divide the pulse length. If the pulses were simultaneously applied with a field gradient of 4.7 mT/m, they all excited a 10-mm slice.

In Figs. 1A–D, the slice profiles of linear phase [see (*6–8*)] 30°, 90°, and 180° pulses are compared. The 180° pulse was used both as inversion pulse (initial magnetization at rest) and as component of a spin-echo sequence (magnetization vector lying along the *y* axis).

Figures 2A and B show the comparison between two minimum phase saturation pulses and two minimum phase inversion pulses, respectively. Because of greater in-slice ripples, the slice profiles due to generalized SLR pulse do not fit the desired rectangular profile as well as those generated by standard SLR pulses.

Concerning the quality of slice profiles, the most interesting results are obtained for pulses whose flip angles run from 50° to 130°. As an example we compare the slice profiles of two 60° pulses (see Fig. 3).

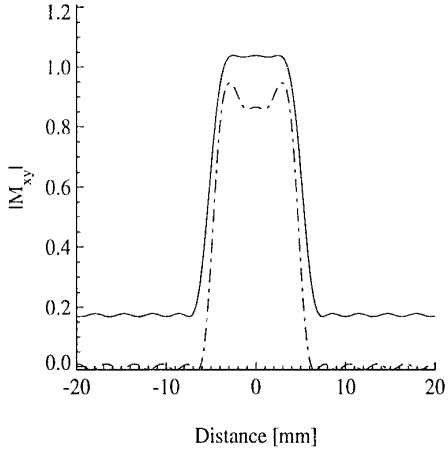


**FIG. 3.** The performance of two linear-phase 60° pulses. The plot compares $|M_{xy}|$ for pulses calculated by using generalized (solid line) and standard (dash–dot line) estimates.

**TABLE 2**
**Standard SLR Pulses: Required, Actual Ripples and Transition Band (TB) Percentage**

| Pulse | Req. $\delta_1^e$ | Act. $\delta_1^e$ | Req. $\delta_2^e$ | Act. $\delta_2^e$ | TB |
|---|---|---|---|---|---|
| 30° | 1.0% | 4.0% | 1.0% | 0.7% | 32% |
| 60° | 1.0% | 9.2% | 1.0% | 1.0% | 23% |
| 90° | 1.0% | 5.6% | 1.0% | 1.3% | 23% |
| 180° | 1.0% | 1.6% | 1.0% | 3.0% | 28% |
| Saturation | 1.0% | 1.4% | 1.0% | 0.8% | 20% |
| Inversion | 1.0% | 0.7% | 1.0% | 0.8% | 27% |

In Tables 2 and 3 results concerning the percentage of transition band and the connection between the input specifications (Req. $\delta_1^e$ and Req. $\delta_2^e$) and the values actually obtained (Act. $\delta_1^e$ and Act. $\delta_2^e$) are summarized. Actual ripples have been calculated as the maximum deviation from the value expected in the desired slice profile.

In all cases, except saturation and inversion pulses, decreased in- and out-of-slice ripples have been found. The wider transition band detected does not make the slice profiles due to generalized SLR pulses unacceptable, the difference not being greater than 17% (*6*).

The specified in-slice and out-of-slice ripples, together with bandwidth and pulse length, determine the transition band: the smaller the ripples are, the wider the transition band is. The RF pulses whose simulated slice profiles were used in Figs. 1–3 were all generated with 1% in-slice and out-of-slice effective ripple amplitudes. An exception is the linear phase 180° pulse and the minimum phase saturation and inversion pulses calculated by using the generalized estimate for the *B* polynomial ripples. They were generated with 1% in-slice and 5% out-of-slice ripples.

In order to compare the behavior of pulses with same flip angle, duration, and bandwidth, but with different values of in-slice and out-of-slice ripples, we generated 90° linear phase pulses with a duration of 3.072 ms and 0.5%, 0.1%, 0.05% and 0.01% ripples using both standard classification and generalized estimate. The results are shown in Tables 4 and 5.

Standard 90° pulses with required ripples amplitude less than 1% have nonequal out-of-slice ripples (256 samples were

**TABLE 3**
**Generalized SLR Pulses: Required, Actual Ripples and Transition Band (TB) Percentage**

| Pulse | Req. $\delta_1^e$ | Act. $\delta_1^e$ | Req. $\delta_2^e$ | Act. $\delta_2^e$ | TB |
|---|---|---|---|---|---|
| 30° | 1.0% | 1.40% | 1.0% | 0.40% | 37% |
| 60° | 1.0% | 0.70% | 1.0% | 0.50% | 40% |
| 90° | 1.0% | 0.07% | 1.0% | 1.30% | 35% |
| 180° | 1.0% | 1.00% | 5.0% | 0.02% | 37% |
| Saturation | 1.0% | 3.70% | 5.0% | 0.20% | 21% |
| Inversion | 1.0% | 2.50% | 5.0% | 0.06% | 29% |

**TABLE 4**
**Standard 90° Linear Phase Pulses**

| Req. $\delta_1^e$ | Act. $\delta_1^e$ | Req. $\delta_2^e$ | Act. $\delta_2^e$ | TB |
|---|---|---|---|---|
| 1.00% | 5.6% | 1.00% | 1.3% | 23% |
| 0.50% | 4.0% | 0.50% | max 1.80% − min 0.70% | 28% |
| 0.10% | 1.3% | 0.10% | max 0.60% − min 0.20% | 39% |
| 0.05% | 0.8% | 0.05% | max 0.35% − min 0.10% | 43% |
| 0.01% | 0.2% | 0.01% | max 0.10% − min 0.02% | 51% |

used for the RF waveform) and the actual ripples are always greater than the required one. This is more evident for in-slice ripples. In case of non-equiripple pulses, the maximum and minimum deviations from one and zero have been calculated. Generalized 90° pulses are equiripples and the actual in-slice ripples are remarkably less than the required one. Out-of-slice ripples are close to the design values. The cost is a 12–27% wider transition band, which is considered to be not too bad (*6*).

The pulses produced by a generalized estimate have a lower value of the energy. In particular, pulses whose flip angle $\phi \in$ [140°, 180°] have an even smaller peak power and shorter Conolly wings.

In Figure 4A we compare the value of the power integral for all three series of linear phase pulses; the percentage of relative power integral is shown in Fig. 4B. For flip angles running from 10° to 40° there is almost no decrease if both 1% in- and out-of-slice ripples are used and even an increase (from 7% to 16%) if generalized 5% are needed. When the flip angle runs from 50° to 130° there is a minimum 11% and a maximum 28% reduction if both 1% in- and out-of-slice ripples are used. There is still a reduction, but only from 5 to 22%, if 5% out-of-slice ripples are required. Finally, for flip angles running from 140° to 180° the decrease changes from 21 to 27% for 1% in-slice and out-of-slice ripples and from 14 to 17% when 5% out-of-slice ripples are required.

In particular, the use of 90° generalized SLR pulses with 1% in-slice and out-of-slice ripples yields a reduction of about 15% in power integral, whereas using 180° generalized SLR pulses with 1% in-slice and 5% out-of-slice ripples permits a reduction in the power integral of about 17%.

In Fig. 5, 180° pulse waveforms are compared. It is worth

**TABLE 5**
**Generalized 90° Linear Phase Pulses**

| Req. $\delta_1^e$ | Act. $\delta_1^e$ | Req. $\delta_2^e$ | Act. $\delta_2^e$ | TB |
|---|---|---|---|---|
| 1.00% | 0.07% | 1.00% | 1.3% | 35% |
| 0.50% | 0.2% | 0.50% | 0.66% | 41% |
| 0.10% | 0.06% | 0.10% | 0.13% | 56% |
| 0.05% | ≈0.001% | 0.05% | 0.04% | 63% |
| 0.01% | ≈0.001% | 0.01% | 0.01% | 78% |

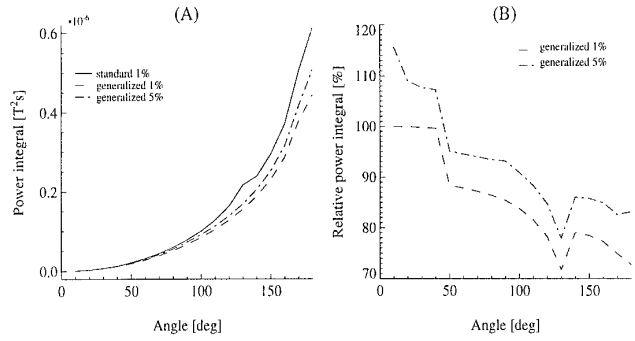


**FIG. 4.** The power integrals calculated for linear phase pulses with different flip angles are compared in (A). Standard (1% out-of-slice ripples) and generalized ripple amplitudes estimate (both in case of 1% and 5% out-of-slice ripples) have been used. In (B) the percentage of relative power integral is shown.

noting that the Conolly wings of the pulse generated using the standard estimate represent roughly 48% of the maximum amplitude, whereas the pulse produced by means of generalized estimate has Conolly wings with only 9.4% of its maximum amplitude. Moreover, their peak amplitude is nearly 9% less than that in the 180° standard SLR pulse. In general, for pulses with flip angles running from 140° to 180° and 5% out-of-slice ripples there is a mean reduction of 8% of the peak amplitude.

## CONCLUSIONS

The simulations we have performed have shown that it is possible to use the pulses generated under the assumption that the initial magnetization is at rest in every sequence (a $\pi$ pulse, for example, can be used both as an inversion pulse and as a spin-echo pulse). Moreover, too wide a transition band in the slice profile due to the use of the generalized estimate can be avoided by increasing the desired out-of-slice ripple amplitude.

The use of generalized estimate allows the avoidance of any previous classification. It even provides pulses with better slice

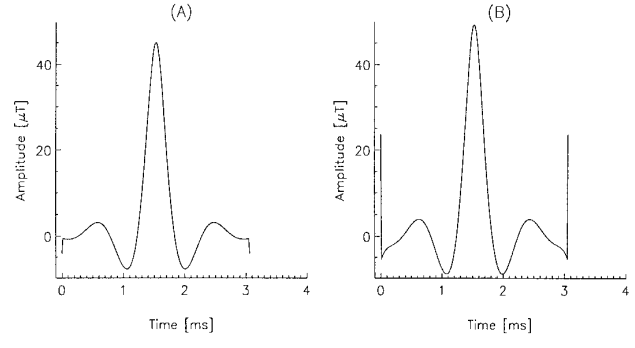


**FIG. 5.** Linear-phase 180° pulses. In (A) the pulse generated making use of generalized estimate is plotted, while the pulse obtained by means of standard ripple amplitude approximation is presented in (B).

profile than those of the standard SLR. These new pulses have smaller out-of-slice ripples and, particularly if the flip angle runs from 140° to 180°, smaller energy and smaller peak power.

## REFERENCES


1. M. Shinnar, S. Eleff, H. Subramanian, and J. S. Leigh, *Magn. Reson. Med.* **12,** 74 (1989).
2. M. Shinnar, L. Bolinger, and J. S. Leigh, *Magn. Reson. Med.* **12,** 81 (1989).
3. M. Shinnar, L. Bolinger, and J. S. Leigh, *Magn. Reson. Med.* **12,** 88 (1989).
4. M. Shinnar, and J. S. Leigh, *Magn. Reson. Med.* **12,** 93 (1989).
5. P. Le Roux, Abstracts of the Society of Magnetic Resonance in Medicine, 7th Annual Meeting, p. 1049, 1989.
6. J. Pauly, P. Le Roux, D. Nishimura, and A. Macovski, *IEEE Trans. Med. Imaging* **10,** 53 (1991).
7. L. R. Rabiner, and B. Gold, ''Theory and Application of Digital Signal Processing,'' Chapter 3, p. 156. Prentice-Hall, Englewood Cliffs, NJ (1975).
8. G. B. Matson, *Magn. Reson. Imaging* **12,** 1205 (1994).